J. Fluid Mech. (2010), *vol.* 651, *pp.* 465–481.
doi:10.1017/S0022112010994160

Multi-layered diffusive convection. Part 2. Dynamics of layer evolution

TAKASHI NOGUCHI† AND HIROSHI NIINO

Ocean Research Institute, The University of Tokyo, Nakano, Tokyo 164-8639, Japan

(Received 25 August 2009; revised 9 December 2009; accepted 18 December 2009; first published online 26 March 2010)

Evolution of layers in an unbounded diffusively stratified two-component fluid and its dynamics are studied by means of a direct numerical simulation (DNS) and an analytical model. The numerical simulation shows that the layers grow by repeating mergings with the neighbouring layers. By analysing the results of the numerical simulation, the mechanism of the merging is examined in detail. Two modes of merging are found to exist: one is the layer vanishing mode and the other is the interface vanishing mode. The vanishings of layers and interfaces are caused by turbulent entrainment at the interfaces. Based on the analysis of the numerical model, a one-dimensional asymmetric entrainment model is proposed. In the model, each layer is assumed to interact with its neighbouring layers through simplified convective entrainment laws. The model is applied to two simple configurations of layers and is proved to reproduce the layer evolutions found in the DNS successfully.

1. Introduction

Diffusive regimes of double-diffusive convection are found in many natural and engineering fluids such as high-latitude oceans (Schmitt 1994), magma chambers (Huppert & Turner 1981) and liquefied gas storage (Zimmerman & Rees 2007). The most striking characteristics of the diffusive convection is to produce layers. It is reported that, once layers are formed, they do not remain steady but evolve with time, both from the laboratory experiments (Shirtcliffe 1969; Linden 1976; Linden & Shirtcliffe 1978) and from observations in the oceans (Neshyba, Neal & Denner 1971). For example, mergings of layer are often observed during their evolutions. However, the dynamics and mechanism of the layer evolutions have not been clarified in a satisfactory manner.

There are several oceanic observations that suggest 'layer splitting' events at the interface (e.g. Neshyba *et al.* 1971). However, such one-dimensional observations are unable to distinguish the true 'layer splitting' from a horizontal advection of a layer patch. If such a splitting process would exist and be active in the oceans, the thickness of the layer is expected to reach an statistical equilibrium value at which the merging and the splitting balance. Thus, whether any layer splitting occurs against layer merging has been of interest (Kelley *et al.* 2003). Stamp *et al.* (1998) speculated that a solitary wave propagating along the diffusive interface may be responsible for such an apparent 'splitting'.

† Present address: Department of Aeronautics and Astronautics, Kyoto University, Yoshida-Honmachi, Sakyo, Kyoto 606-8501, Japan. Email address for correspondence: noguchi@kuaero.kyoto-u.ac.jp

Part 1 of the present paper (Noguchi & Niino 2010), studied diffusive convection in an unbounded diffusively stratified two-component fluid by a DNS and found formation of layers. Each layer consists of a convective mixed layer, which is sandwiched by diffusive interfaces with a sharp density gradient. As time elapses, each layer merges with its adjacent layers repeatedly, and the layer thickness increases on average. Now, important questions on the dynamical aspect of layers are (i) how layers merge, (ii) what controls the merging process and (iii) whether the merging is inevitable or not.

Dynamics of a layer growth have been studied by a mathematical model that represent evolutions of layer thickness and components based on empirical flux laws. Huppert & Linden (1979) studied a problem of stratified fluid heated from bottom and proposed a model that can simulate layer productions and mergings. They found a reasonable agreement between the predicted layer evolution and their laboratory experiment, although the migration of the interface is ignored in their model. For similar configuration (solar pond problem), Zangrando & Fernando (1991) introduced the effects of migrating interface due to entrainment through interfaces, and found an equilibrium state. This entrainment–detrainment equilibrium is confirmed by data from laboratory experiments.

The aim of the present study is to clarify the dynamics of the evolution of layers in multi-layer configuration by constructing a model that includes both migration and dissipation of interfaces. In § 2, a brief description of the direct numerical model used for the diffusive convection in multi-layered stratification is made and the temporal behaviour of the layer is presented. In § 3, the structure of the multi-layered convection is analysed, and several qualitative rules on the movement of layer interfaces are derived. In § 4, a mechanistic model that describes the evolution of layers is proposed. The model will be shown to reproduce the merging processes found in the DNS in a satisfactory manner. A discussion of the results is presented in § 5. Summary and conclusions are given in § 6.

2. Numerical experiment

2.1. *Numerical model*

In the present paper, the results of DNS as described in Noguchi & Niino (2010) is analysed. We will here give a brief description of the DNS. Readers are referred to Noguchi and Niino for their details.

The numerical model solves governing equations for two-dimensional incompressible convective motions due to double-diffusive effect. The fluid is initially at rest and is diffusively stratified with faster and slower diffusing component T and S, respectively. The gradient ratio

$$\gamma = -\frac{\partial \overline{\rho_T}/\partial z}{\partial \overline{\rho_S}/\partial z}$$

is positive and less than 1, where $\overline{\rho_T}$ and $\overline{\rho_S}$ denote contributions of T and S to the basic density field, respectively, and $-\partial \overline{\rho_S}/\partial z > \partial \overline{\rho_T}/\partial z > 0$. After a suitable scaling, the governing equations in non-dimensional form are given by

$$\left(\frac{\partial}{\partial t} - Pr\nabla^2\right)\nabla^2\psi = -J(\psi, \nabla^2\psi) - Pr\left(\frac{\partial T}{\partial x} - \frac{1}{\gamma}\frac{\partial S}{\partial x}\right), \tag{2.1}$$

$$\left(\frac{\partial}{\partial t} - \nabla^2\right)T = -J(\psi, T) - \frac{\partial \psi}{\partial x}, \tag{2.2}$$

$$\left(\frac{\partial}{\partial t} - \tau\nabla^2\right)S = -J(\psi, S) - \frac{\partial \psi}{\partial x}, \tag{2.3}$$

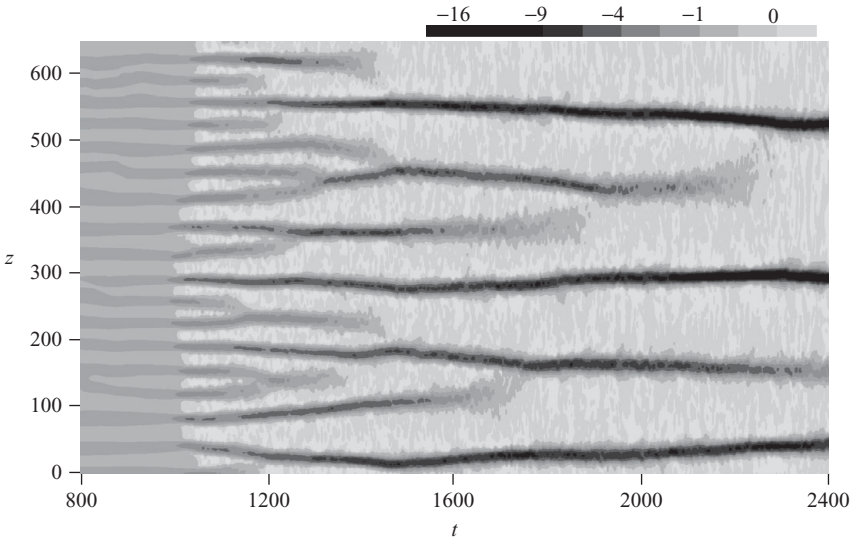

FIGURE 1. Time-height cross-section of horizontally averaged vertical density gradient for $\gamma = 0.88$. The time interval between 800 and 2400 is shown. The multi-layered convective motions begin at $t \sim 1000$.

where ψ is the stream function and $J(a, b)$ is Jacobian. Note that the length is scaled by an intrinsic length scale $\delta = |g\alpha\overline{T_z}/\kappa_T\nu|^{-1/4}$, where g is the gravity acceleration, α the coefficient of contraction due to component T, $\overline{T_z}$ the basic vertical gradient of T, κ_T the diffusivity of component T and ν the kinematic viscosity. The non-dimensional parameters that appear in (2.1)–(2.3) are Prandtl number $Pr = \nu/\kappa_T$, the diffusivity ratio $\tau = \kappa_S/\kappa_T$ and γ, where κ_S is the diffusivity of component S. An aqueous salt-heat system ($Pr = 7$ and $\tau = 0.01$) is considered in the present study.

The calculation domain is $632\delta \times 632\delta$ and periodic boundary conditions are imposed on both vertical and horizontal boundaries. White noise of T with tiny amplitude are used as initial disturbance. In this paper we will examine the cases of $\gamma = 0.88$ and 0.89, which are linearly unstable to diffusive convection (see Noguchi & Niino 2010 for linear stability analysis).

2.2. *Simulated evolution of layers*

Figure 1 shows the time evolution of vertical density gradient, which is averaged horizontally over the whole calculation domain for $\gamma = 0.88$ after $t = 800$ when the layer structure is established. Eighteen alternations of large and small vertical density gradients are seen at $t \sim 800$. Convective motions commence at $t \sim 1000$ and the density gradient within the layer becomes very small due to their efficient mixing. Once formed, layers increase their thickness by repeating mergings with adjacent layers and result in four layers with somewhat uneven thickness by $t \sim 2400$.

The thickness of the interfaces that separate the convective mixed layers is about 10 at $t \sim 800$. It then slowly increases with time and becomes 15 at $t \sim 2400$. Although the interface thickness shown in the figure may be influenced by the horizontal inhomogeneity of the interface at later time, the change of the interface thickness with time is much smaller than that of layer thickness. The density gradient at the interface also seems to increase with time.

When γ is increased to 0.89, layers grow much quicker since this case is more supercritical (figure 2). About 30 layers exist at $t = 150$. These layers repeat

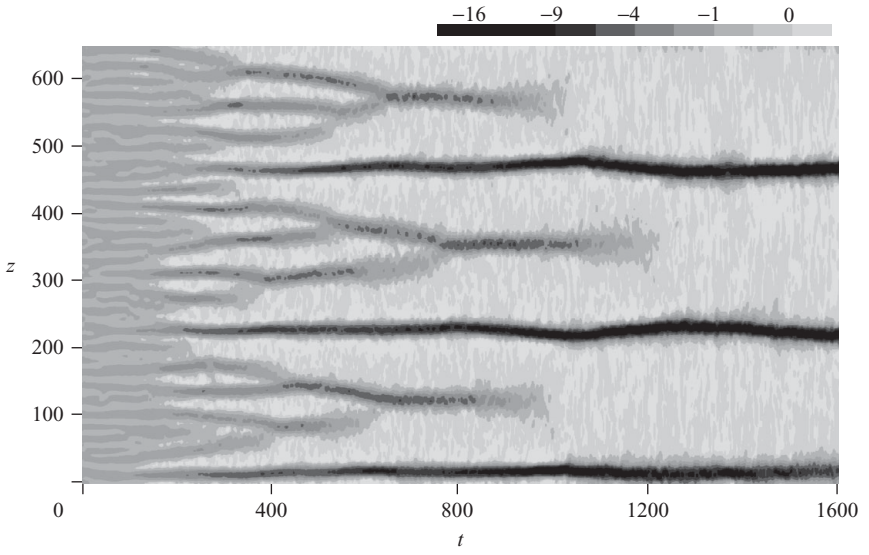

FIGURE 2. Time-height cross-section of horizontally averaged vertical density gradient for $\gamma = 0.89$. The multi-layered convective motions begin at $t \sim 150$.

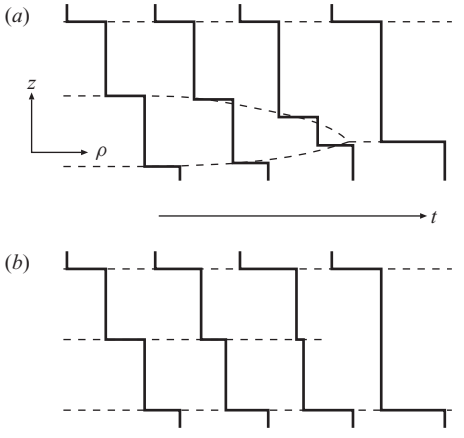

FIGURE 3. The two modes of layer merging: (*a*) layer vanishing mode, (*b*) interface vanishing mode.

mergings much more quickly than they do for $\gamma = 0.88$ and leave only 3 layers by $t \sim 1600$.

Both figures 1 and 2 show that there are two modes of layer merging: a layer vanishing mode and a interface vanishing mode. Figure 3 illustrates these modes schematically. In the layer vanishing mode (figure 3*a*), a layer gradually decreases its thickness and finally vanishes. If one looks at the interfaces, this mode appears as the merging of two adjacent interfaces. In the interface vanishing mode, on the other hand, density difference at the interface decreases with time and finally vanishes (figure 3*b*), so that the interface disappears. Figures 1 and 2 show that these two modes are not exclusive of each other and mergings in general take place in some mixed way between the two extreme modes.

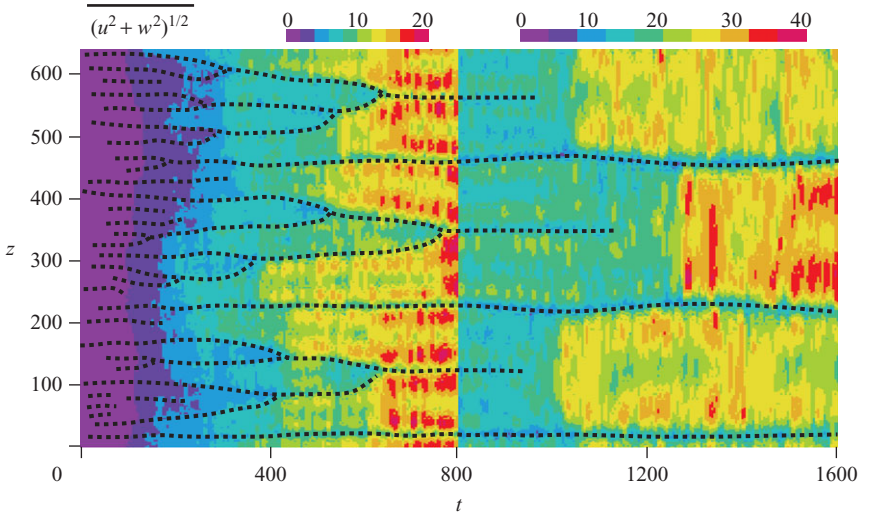

FIGURE 4. Time-height cross-section of square root of horizontally averaged kinetic energy density, for $\gamma = 0.89$. Note that the colour shading is rescaled by a factor of 2 at $t = 800$. Layer interfaces are indicated by dotted lines.

3. Physical interpretation of layer merging

In this section, we examine several statistical quantities associated with the simulated convective motions to clarify the possible factors that govern the migration and vanishing of interfaces. For this purpose, the following assumptions are made: (*a*) The migration and vanishing of the interfaces are controlled by convective motions within the mixed layer, and (*b*) convective motions are statistically homogeneous throughout each layer.

3.1. *Kinetic energy difference*

First, we examine the kinetic energy. Figure 4 shows the time-height cross-section of square root of horizontally averaged kinetic energy density, $(\overline{u^2 + w^2})^{1/2}$, where u and w are horizontal and vertical velocities, respectively, and the overbar denotes the horizontal average over the calculation domain. Several empirical rules can be deduced from this figure:

(*a*) Kinetic energy at the interfaces is always very small. This implies that the motion is strongly suppressed by the sharp stable density gradient there.

(*b*) The migration velocity of the interfaces is typically about 10 times as small as that of the fluid motion within the layers.

(*c*) Motions within the layers become vigorous as the layer thickness increases.

(*d*) An interface moves from the layer of larger kinetic energy towards that of smaller kinetic energy.

The empirical rule (*d*) can be explained qualitatively in terms of competition of turbulent entrainment from both sides of the interface (figure 5): From either side of an interface, turbulent convective eddies try to entrain fluid from the other side of the interface. If the kinetic energy on one side of the interface is different from that on the other side, the layer with larger kinetic energy entrains more fluid than the other layer does. To satisfy the mass conservation, the interface must move towards the layer of smaller kinetic energy.

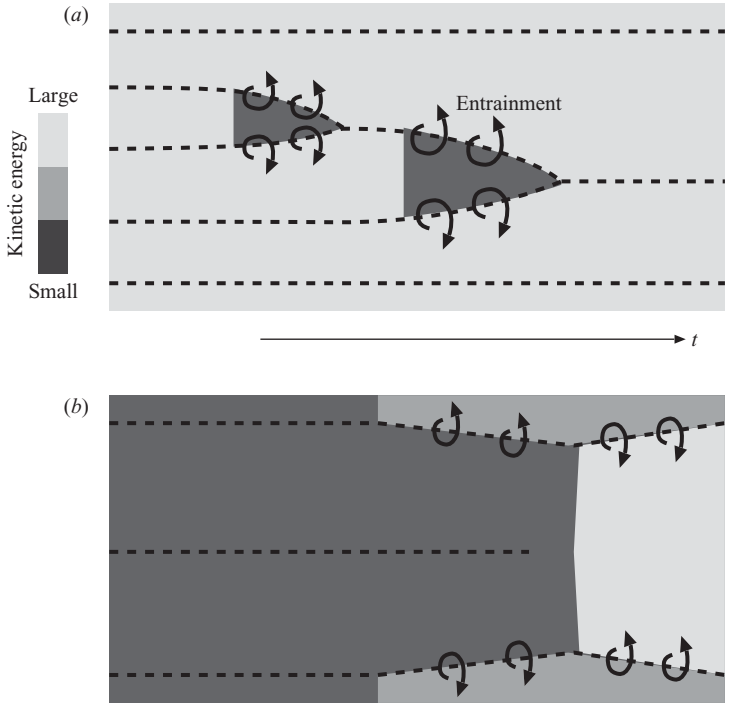

FIGURE 5. Schematics of the relation between the kinetic energy distribution and the change of the layer thickness: (*a*) layer vanishing mode, (*b*) interface vanishing mode. Grey scale denotes the magnitude of kinetic energy averaged within a layer.

For the layer vanishing mode (figure 5*a*), the fluid inside the thinner layer, which has smaller kinetic energy according to rule (*c*), is entrained by the thicker layer and eventually disappears. The generality of rule (*c*) is also seen in the interface vanishing mode (figure 5*b*). After an interface vanishes, the layer thickness doubles. This results in an increase of kinetic energy, and consequently an increase of entrainment. Their dependencies on the layer thickness d can be explained by the fact that a Rayleigh number defined for each layer is expressed as

$$Ra = \frac{g\alpha\overline{T_z}d^4}{\kappa_T \nu} = \frac{d^4}{\delta^4}$$

and that in general velocity of convective motion is a monotonic increasing function of Ra.

3.2. *Skewness of vertical velocity*

For the interface vanishing mode, a vertical asymmetry of the layer structure appears to be important. Let us look at figures 1 and 2, for example. When an interface disappears, the density gap of the interface weakens while the density gaps across the neighbouring interfaces show significant increase. This is schematically shown in figure 5(*b*). The vertical asymmetry of convective motions can be detected by calculating the skewness of vertical velocity S_w defined by

$$S_w \equiv \frac{\overline{w^3}}{\overline{w^2}^{3/2}}. \tag{3.1}$$

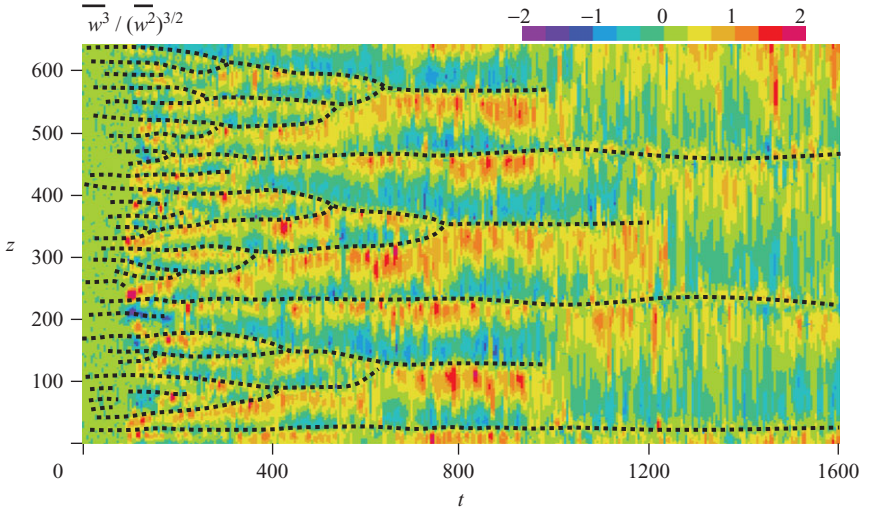

FIGURE 6. Time-height cross-section of the skewness of w, for $\gamma = 0.89$.

Before starting the analysis of the present case, let us briefly review the characteristics of S_w in the convective layer, according to Moeng & Rotunno (1990). They performed DNS of convections in a fluid layer with symmetric and asymmetric thermal forcing at the boundaries. When the forcing is symmetric, which means the fluid is cooled from top and heated from bottom at the same rate, S_w is antisymmetric with respect to the middle height of the layer, and has a positive peak near the top of the layer and a negative peak near the bottom. When the forcing is asymmetric, on the other hand, which means heating is imposed only at the bottom, S_w is positive at all height and has a peak near the top. This can be interpreted in terms of plume activities as follows: When the forcing is symmetric, upward and downward plumes emerges with statistically equal strength and frequency. The upward (downward) plume accelerated by the positive (negative) buoyancy in the plumes becomes largest near the top (bottom). When the forcing is only at the bottom, on the other hand, stronger upward plumes occupy small fraction of the layer, and weaker compensating downward plumes the rest. Thus, S_w is positive everywhere.

Figure 6 shows the time evolution of S_w in the present system. Here we focus on the behaviour of the skewness before the interfaces disappear (e.g. $z \sim 120$ and 570 at $t \sim 1000$, and $z \sim 350$ at $t \sim 1200$). Well before the interfaces start to disappear, the skewness in the adjacent layers is antisymmetric with respect to the middle height of the layers. When the interfaces start to weaken, however, the skewness in the upper (lower) layer starts to be dominated by negative (positive) values. This shows that downward (upward) plumes start to dominate in the upper (lower) layer. These plumes, trying to penetrate the interface, entrain actively the fluid on the other side and eventually eliminate the density contrast between the two layers. This process is schematically illustrated in figure 7.

4. Asymmetric entrainment model

Based on the observation presented in the previous section, we propose here a mechanistic model of the evolution of layers. In this model we regard each convective layer bounded by two diffusive interfaces as a discrete element, and the whole

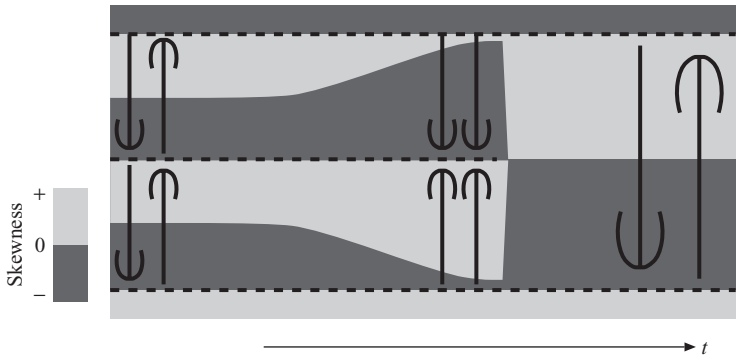

FIGURE 7. Schematic of the relation between the skewness of w and the plumes during the interface vanishing.

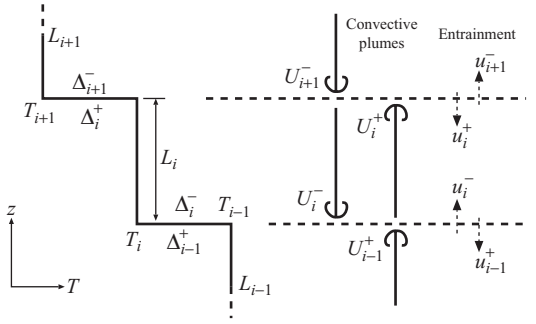

FIGURE 8. Schematic illustration of the asymmetric entrainment model. T is the temperature of layer, Δ the temperature difference at the interface, L the thickness of layer, U the velocity of plumes and u the entrainment velocity. The subscripts denote the number of layer, and the superscripts + and − for the values at the top and bottom of the layer, respectively.

stack of convective layers as an one-dimensional array of such elements, in which each element interacts only with its nearest neighbours. The characteristics of the interaction is assumed to depend only on local properties. Figure 8 illustrates the present mechanistic model schematically.

The assumptions made in the model are the followings:

(*a*) Each layer is well mixed by turbulent convections, so that both temperature and salinity are homogeneous throughout the layer.

(*b*) Density difference between layers is proportional to their temperature difference. (Therefore salinity difference is also proportional to temperature difference.)

(*c*) Convective plumes have density deficit (or surplus) proportional to the temperature difference at the interface from which they originate.

(*d*) Plumes are accelerated at a constant buoyancy prescribed by the density deficit (or surplus) during their ascent (descent). Viscous retardation is ignored.

(*e*) Plumes ascent or descent without mixing with ambient fluid.

(*f*) Plumes impinging into an interface entrain fluid from the other side through the interface.

(*g*) Aspect ratio of the convective plumes is of the order of unity, so that the vertical and horizontal velocity scales are similar.

Let us express these assumptions in a mathematical form. Consider a plume which originates from the bottom of the ith layer (figure 8). The ith layer has a thickness

L_i and temperature T_i, respectively. An integration of the buoyancy acceleration over the layer thickness gives the final velocity of the ascending plume near the top of the layer,

$$U_i^+ = A(\Delta_i^- L_i)^{1/2}, \tag{4.1}$$

and that of descending plume near the bottom of the layer,

$$U_i^- = A(\Delta_i^+ L_i)^{1/2}, \tag{4.2}$$

where the superscripts + and − stand for the values at the top and bottom of the layer, respectively. A is a constant coefficient, $\Delta_i^+ = T_i - T_{i+1}$ and $\Delta_i^- = T_{i-1} - T_i$. The entrainment velocity u_i, which is defined as the volume entrainment rate, is assumed to be given by the plume impingement velocity as

$$u_i^+ = B\frac{(U_i^+)^3}{\Delta_i^+ L_i} \tag{4.3}$$

and

$$u_i^- = B\frac{(U_i^-)^3}{\Delta_i^- L_i}, \tag{4.4}$$

where B is a coefficient of the entrainment efficiency and is assumed to be a constant. Note that this equation has a similar form as Turner's relation based on Richardson number Ri (Turner 1965),

$$\frac{u}{U} \sim Ri^{-1} \sim \frac{U^2}{\Delta \cdot L}. \tag{4.5}$$

Substituting (4.1) into (4.3), one obtains

$$u_i^+ = A^3 B\frac{(\Delta_i^-)^{3/2} L_i^{1/2}}{\Delta_i^+} \tag{4.6}$$

and similarly,

$$u_i^- = A^3 B\frac{(\Delta_i^+)^{3/2} L_i^{1/2}}{\Delta_i^-}. \tag{4.7}$$

Under these assumptions, the conservation laws for mass and heat for ith layer,

$$\frac{\mathrm{d}L_i}{\mathrm{d}t} = u_i^+ + u_i^- - u_{i-1}^+ - u_{i+1}^-, \tag{4.8}$$

$$\frac{\mathrm{d}(L_i T_i)}{\mathrm{d}t} = u_i^+ T_{i+1} + u_i^- T_{i-1} - u_{i-1}^+ T_i - u_{i+1}^- T_i, \tag{4.9}$$

can be rewritten by use of (4.6) and (4.7), as

$$\frac{\mathrm{d}L_i}{\mathrm{d}t} = \left[\frac{(\Delta_i^-)^{3/2} L_i^{1/2} - (\Delta_{i+1}^+)^{3/2} L_{i+1}^{1/2}}{\Delta_i^+} + \frac{(\Delta_i^+)^{3/2} L_i^{1/2} - (\Delta_{i-1}^-)^{3/2} L_{i-1}^{1/2}}{\Delta_i^-}\right], \tag{4.10}$$

$$\frac{\mathrm{d}T_i}{\mathrm{d}t} = \left[-(\Delta_i^-)^{3/2} + (\Delta_i^+)^{3/2}\right](L_i)^{-1/2}, \tag{4.11}$$

where $\mathrm{d}t$ has been rescaled to accommodate the factor of $A^3 B$, and the relations $\Delta_{i-1}^+ = \Delta_i^-$ and $\Delta_{i+1}^- = \Delta_i^+$ has been used. Now, given an initial condition, we can calculate the evolution of the layers using (4.10) and (4.11). The present model will be henceforth referred to as *asymmetric entrainment model*. In the following subsections, we will demonstrate the performance of the model for two simple configurations.

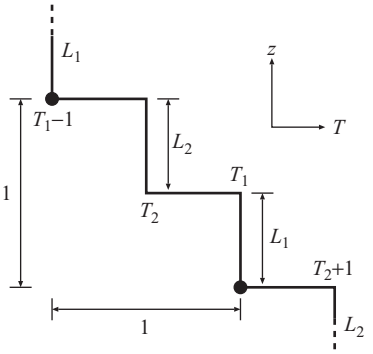

FIGURE 9. A periodic two-layer configuration. Solid circles denote the boundary of a period.

4.1. *Periodic two-layer system*

The first example we consider is the simplest configuration in which a two-layer system is repeated periodically (figure 9). Let the temperature difference and depth for one cycle of the two-layer system be unity. If the temperature and depth of the lower layer are denoted by T_1 and L_1, then those of the upper layer are given by T_2 and $L_2 = 1 - L_1$, respectively. For this configuration, (4.10) and (4.11) of the asymmetric entrainment model are reduced to

$$\frac{\mathrm{d}L_1}{\mathrm{d}t} = \left[\frac{(T_1 - T_2)^{3/2}}{T_2 - T_1 + 1} + \frac{(T_2 - T_1 + 1)^{3/2}}{T_1 - T_2}\right]\left(L_1^{1/2} - L_2^{1/2}\right) \tag{4.12}$$

and

$$\frac{\mathrm{d}T_1}{\mathrm{d}t} = \left[-(T_2 - T_1 + 1)^{3/2} + (T_1 - T_2)^{3/2}\right](L_1)^{-1/2}, \tag{4.13}$$

$$\frac{\mathrm{d}T_2}{\mathrm{d}t} = \left[-(T_1 - T_2)^{3/2} + (T_2 - T_1 + 1)^{3/2}\right](L_2)^{-1/2}. \tag{4.14}$$

If new variables defined by

$$\Delta = T_1 - T_2, \tag{4.15}$$

$$L = L_1 \tag{4.16}$$

are introduced, (4.12)–(4.14) are further reduced to

$$\frac{\mathrm{d}L}{\mathrm{d}t} = \left[\frac{\Delta^{3/2}}{1 - \Delta} + \frac{(1 - \Delta)^{3/2}}{\Delta}\right]\left(L^{1/2} - (1 - L)^{1/2}\right), \tag{4.17}$$

$$\frac{\mathrm{d}\Delta}{\mathrm{d}t} = \left[\Delta^{3/2} - (1 - \Delta)^{3/2}\right]\left(L^{-1/2} + (1 - L)^{-1/2}\right). \tag{4.18}$$

Equations (4.17)–(4.18) constitutes a two-dimensional dynamical system. When an initial condition is given for L and Δ, we can calculate the time evolution of the two-layer system based on (4.17)–(4.18). Since these equations are nonlinear, however, we need to solve them numerically.

Figure 10 shows the evolution of Δ and L on the phase plane (Δ, L). The open circle at the centre designates the source point and the four solid circle at the corners the sink points. Note that only the point $(\Delta, L) = (1/2, 1/2)$ is the steady-state solution of (4.17)–(4.18), but it is unstable to infinitesimal perturbations. As (4.17)–(4.18) are defined only in the interior of the phase plane, the arrows on the boundary $\Delta = 0, 1/2$

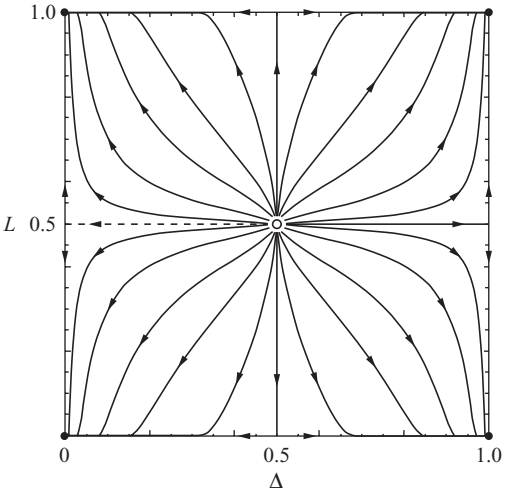

FIGURE 10. Time evolution of periodic two-layer system (see (4.17) and (4.18)) plotted on the phase plane (Δ, L). The open circle at the centre denotes source point and the four solid circles at the corners denote sink points. The dashed orbit is for the later explanation.

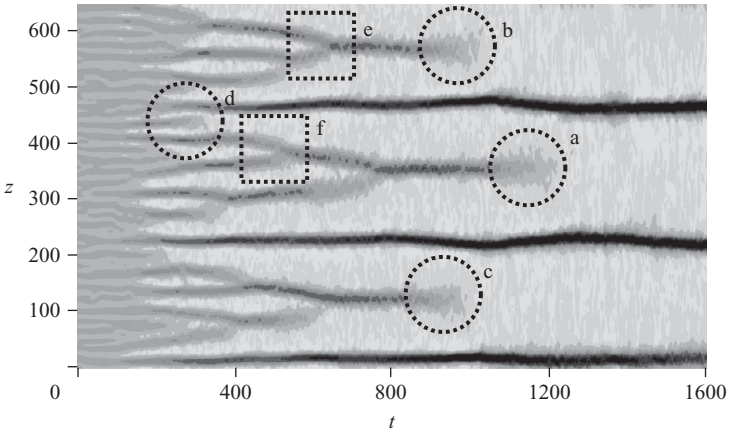

FIGURE 11. The target events for testing the applicability of the asymmetric entrainment model: a–d the interface vanishing mode, and e–f the layer vanishing mode. The background is the same as figure 2.

and $L = 0, 1$ are drawn in the asymptotic sense: a state close to boundary evolves towards the direction of the arrow.

When L $(=L_1)$ is greater than $1/2$, it increases with time. Eventually layer 1 fills up the whole layer and layer 2 vanishes. When L is less than $1/2$, on the other hand, it decreases with time and layer 1 eventually vanishes. These behaviours correspond to the layer vanishing mode. Similarly, when the temperature difference Δ between layers 1 and 2 is greater than $1/2$, it increases with time and eventually the temperature difference at the top of layer 1 vanishes, while when Δ is less than $1/2$, the temperature difference at the bottom of layer 1 vanishes. This corresponds to the interface vanishing mode.

Let us apply the solution in the two-layer system to the interface vanishing event in the DNS. For the four events of interface vanishing shown in figure 11, their scaled

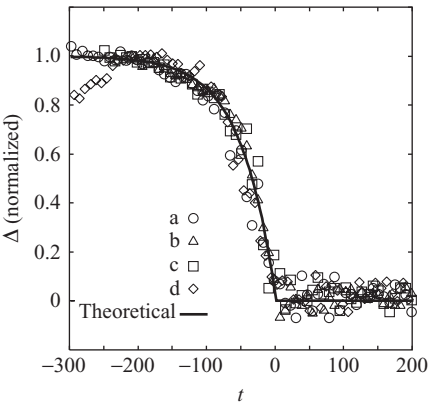

FIGURE 12. Time evolution of temperature difference at the interface, during the four events of interface vanishing as shown in figure 11. Temperature differences are normalized by their value at 200 non-dimensional time before the vanishings of interfaces. The solid curve shows the numerical solution of the periodic two-layer model. Fitting parameter is $A^3B = 3.3 \times 10^{-3}$.

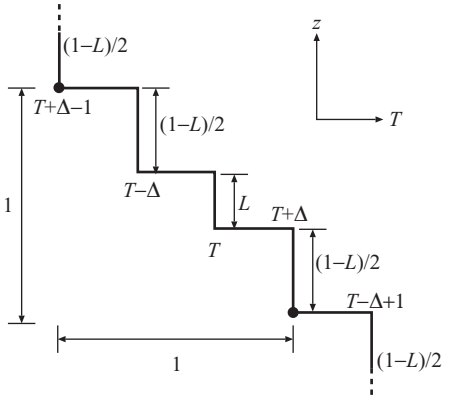

FIGURE 13. A periodic three-layer configuration. Solid circles indicate the boundary of a period.

time evolution of temperature difference across the interface is shown in figure 12. The superposed curve shows the numerical solution of the periodic two-layer system with the initial condition of $(\Delta, L) = ((1/2) - \delta, 1/2)$, where δ is a small positive number, so that the solution moves along the dashed orbit in figure 10. It should be noted that Δ attains 0 within a finite time. Data from the DNS and the curve predicted by the two-layer model are shown by matching the time at which Δ attains 0, and by normalizing the temperature difference by the value at 200 non-dimensional time before the vanishing of interface. A least square fitting of the theoretical curve to the data points gives $A^3B = 3.3 \times 10^{-3}$, which is the normalization factor of the time scale in (4.10) and (4.11). The agreement between the theory and the DNS is very satisfactory. The departure of Δ from the initial value grows almost exponentially with time, and eventually Δ vanishes. Note that the fluctuations of the data points in the DNS after the vanishing of Δ is caused by the passage of plumes through the height of the disappeared interface.

4.2. *Periodic three-layer system*

Next, we proceed to a periodic three-layer configuration (figure 13). In such a configuration, at least four degrees of freedom are needed to describe the evolution

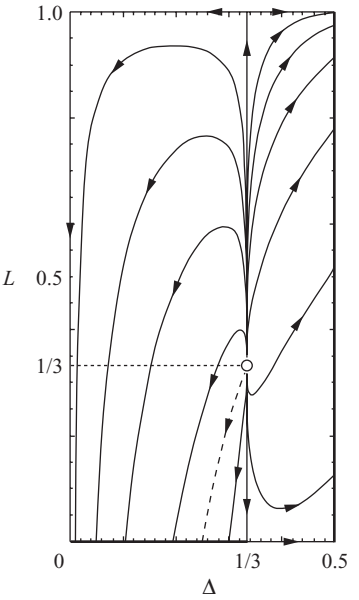

FIGURE 14. Time evolution of the periodic three-layer system (see (4.19) and (4.20)) plotted on the phase plane (Δ, L). The open circle at $(\Delta, L) = (1/3, 1/3)$ denotes the source point and the thick lines on the sides $\Delta = 1/2$ and $L = 0$ denote the sink. Note that the arrows on the thin lines $\Delta = 0, 1/3$ and $L = 0, 1$ are drawn in the asymptotic sense: a point close to each line moves to the direction of the arrow. For the explanation of the dashed orbit that terminates at $(1/4, 0)$, see the text.

of the system and this complicates the analysis. To keep the analysis simple, an additional symmetric constraint is imposed: The top and bottom layers always have the same depth and the temperature differences at the top and the bottom interfaces of the middle layer are equal. This constraint reduces the degree of freedom to two.

Again let the temperature difference and depth for one cycle of the three-layer system be unity. When the temperature and depth of the middle layer are denoted by T and L, respectively, the temperature of the upper and lower layers, under the constraints mentioned above, are given by $T - \Delta$, $T + \Delta$, respectively, and the depth of the upper and lower layers by $(1 - L)/2$, where Δ is the temperature difference across the interfaces at the top and bottom of the middle layer.

For this configuration, (4.10) and (4.11) are reduced to

$$\frac{\mathrm{d}L}{\mathrm{d}t} = 2\left[\Delta^{1/2}L^{1/2} - \frac{(1-2\Delta)^{3/2}}{\Delta}\left(\frac{1-L}{2}\right)^{1/2}\right], \tag{4.19}$$

$$\frac{\mathrm{d}\Delta}{\mathrm{d}t} = \left[\Delta^{3/2} - (1-2\Delta)^{3/2}\right]\left(\frac{1-L}{2}\right)^{-1/2}. \tag{4.20}$$

Figure 14 gives the evolution of Δ and L on the phase plane (Δ, L). The open circle at $(\Delta, L) = (1/3, 1/3)$ denotes the source point at which all the layers have equal layer depths and temperature differences. The point is the only non-zero steady-state solution of (4.17)–(4.18), but it is again unstable to infinitesimal perturbations. The phase orbits terminate at the thick lines on the sides of the box, which are the sink of the system. At the final point of solutions on the sink line at $\Delta = 0.5$, the temperature difference at the top of the upper layer (the bottom of the lower layer)

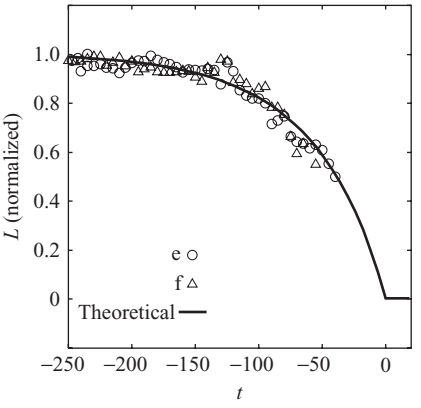

FIGURE 15. Time evolution of layer thickness, before and after the two events of layer vanishing shown in figure 11. Layer thickness is normalized by their value at 150 non-dimensional time before the merging. The solid curve shows the numerical solution of periodic three layer system (see the text for conditions). The fitting parameter A^3B is the same as in figure 12.

vanishes, and on the sink line at $L=0$ the thickness of the middle layer vanishes. In both cases, the system shifts to the two-layer configuration, so that the further evolution can be calculated by means of the periodic two-layer system described in the previous subsection. It is also noted that unlike the solution of the two-layer system, the change in the layer thickness is not always monotonic in the three-layer system.

When the temperature difference Δ at the top and the bottom of the middle layer is less than 1/3, Δ decreases with time and at the same time the layer thickness L vanishes. This corresponds to the layer vanishing mode. On the other hand, when Δ is greater than 1/3, Δ increases with time until the interface at the top of the upper layer (which is also the interface at the bottom of the lower layer, due to periodicity) disappears, which corresponds to the interface vanishing mode.

Let us compare a solution of the three-layer system with the results of the DNS. Figure 15 shows the time evolution of layer thickness during the two events of layer vanishing as shown in figure 11. Layer thickness observed at various time in the DNS are shown by marks with a theoretical curve obtained from the three-layer model, where the layer thickness is normalized by the value at 150 non-dimensional time before the vanishing. The value of A^3B to scale the time is the same as that used in the periodic two-layer system. This demonstrates the universality of the model. The lack of points near $t=0$ is due to difficulties in a precise determination of L: As L becomes small, the fractional change of the thickness becomes large due to the fluctuation of the interface.

Some preliminary calculations show that the time rate of change of L varies substantially from orbit to orbit in the neighbourhood of $\Delta=0$. The curve shown in figure 15 corresponds to the orbit shown by the dashed curve in figure 14. To obtain the orbit with the final point of $(L, \Delta)=(0, 1/4)$, (4.19) and (4.20) is integrated in reverse direction from the point $(L, \Delta)=(10^{-3}, 1/4)$ to the neighbourhood of the source point. The final point $(L, \Delta)=(0, 1/4)$ corresponds to a two-layer system of equal thickness and temperature difference. This corresponds to the final state in the two layer-vanishing events in the DNS (figure 11, modes e and f).

5. Discussion

The asymmetric entrainment model proposed in this paper has been shown to successfully reproduce the results of the DNS. This indicates that the essential aspect of the merging event in layers driven by diffusive convection can be reasonably understood within the framework of a simple one-dimensional discrete model.

According to the results of the asymmetric entrainment model as well as those of the DNS, the layer merging is an essential and inevitable feature of the multi-layered convective system. In the periodic two-layer example, the equilibrium is attained only when the two layers are exactly equivalent to each other, but this state is unstable to infinitesimal disturbances.

The results of the entrainment model in periodic two- and three-layer configurations suggest that layers are destined to merge with its neighbour, although this is not proved in more general situation. If it is true, once the first round of merging process is completed, the geometry of the problem become almost similar to the initial state before the merging, except that the vertical scale is now doubled. Moreover, the time evolutions of Δ and L observed at the different time and location in the DNS show a surprising similarity if the time is shifted and the thickness is scaled properly (figures 12 and 15). These facts demonstrate that the evolution of multi-layered convective system is likely to be self-similar and thus the layers are expected to evolve perpetually with time.

It is also noted that the present model assumes that the plumes are driven mainly by forcing of faster diffusing component (e.g. temperature in heat-salt system), and the diffusive flux of slower diffusing component is ignored. This may be justified for a heat-salt system for which $\tau = 10^{-2}$, but may not for a sugar–salt system for which $\tau = 1/3$.

If the dynamics considered in the present layer model includes all the important physics contained in the DNS, one would expect that no layer splitting event is likely to occur in a multi-layered diffusive convection. In fact it is not possible for a new layer to form in the present model: Suppose a thin layer of thickness L is produced between preexisting layers through layer splitting. Entrainment caused by this layer would be much weaker than entrainment from adjacent preexisting layers. Thus the new layer would reduce its thickness and would be eventually absorbed into one of the adjacent layers.

Furthermore, our model suggests that there seems to be no stable steady configuration of layers. Huppert (1971) found that a three layer system in which a thin layer is placed in between two semi-infinite stratified layers can be steady or oscillatory, while Zangrando & Fernando (1991) found an equilibrium state of a single convective layer topped with an semi-infinite stratified layer. However, under the present multi-layer configuration in which stratified layer is absent, the layers does not seem to have a steady state solution which is stable to infinitesimal perturbation.

In the DNS, the layers merge successively and eventually one deep layer fills the whole vertical span of the calculation domain. If the vertical size of the calculation domain would be infinite, this experiment would yield a layer with an infinite depth after infinite time. According to field observations in oceans, however, the vertical scale of oceanic staircases seems to be less than a certain value. Thus, in the oceans there must be some other mechanisms that limit the growth of layers, such as horizontal advection of layer, breaking of internal gravity waves at the interface (Stamp *et al.* 1998), or some kind of two- or three-dimensional process which are not incorporated either in the present DNS or in the one-dimensional model.

6. Summary and conclusions

Evolution of layers in an unbounded diffusively stratified two-component fluid is studied by means of a DNS and an analytical model. The DNS shows that the layers grow by repeating merging with the neighbouring layers. It is also found that there are two modes of merging: the layer vanishing mode and the interface vanishing mode.

A statistical analysis based on kinetic energy and skewness of vertical velocity gives the following empirical rules on the behaviour of the layers: (i) an interface moves from the layer with larger kinetic energy to that with smaller kinetic energy; (ii) when an interface starts to weaken, the skewness in the upper (lower) layer starts to be dominated by negative (positive) values, which indicates that upward (downward) plumes become dominant. These rules suggest that the vanishing of layers and interfaces are caused by turbulent entrainment associated with plumes impinging on the interfaces.

Based on the above analysis, an asymmetric entrainment model is proposed. The model consists of one-dimensional array of layers each of which interacts with its nearest neighbours through entrainment at the interfaces. The entrainment is assumed to be caused by impingements of thermally driven convective plumes onto the interface and to obey a simplified convective entrainment law. The asymmetric entrainment model applied to two simple configuration of layers such as periodic two-layer and three-layer systems turns out to reproduce the two modes of mergers rather nicely. Furthermore, the evolutions of the layer vanishing modes and the interface vanishing modes obtained in the DNS prove to be well described by the asymmetric entrainment model.

The present asymmetric entrainment model assumes that the diffusivity ratio τ is very small. It is of interest to examine the effect of τ on the behaviour of the layers by means of a DNS and to extend the asymmetric entrainment model to a more general case in which τ is not very small. This is left for a future study.

The authors thank Professor Ryuji Kimura for many fruitful discussions and insights. T. Noguchi would also like to acknowledge the financial assistance of cooperative research program of Ocean Research Institute, the University of Tokyo.

REFERENCES

Huppert, H. E. 1971 On the stability of a series of double-diffusive layers. *Deep Sea Res.* **18**, 1005–1021.

Huppert, H. E. & Linden, P. F. 1979 On heating a stable salinity gradient from below. *J. Fluid Mech.* **95**, 431–464.

Huppert, H. E. & Turner, J. S. 1981 A laboratory model of a replenished magma chamber. *Earth Planet. Sci. Lett.* **54**, 144–172.

Kelley, D. E., Fernando, H. J. S., Gargett, A. E., Tanny, J. & Özsoy, E. 2003 The diffusive regime of double-diffusive convection. *Prog. Oceanogr.* **56**, 461–481.

Linden, P. F. 1976 The formation and destruction of fine-structure by double diffusive processes. *Deep Sea Res.* **23**, 895–908.

Linden, P. F. & Shirtcliffe, T. G. L. 1978 The diffusive interface in double-diffusive convection. *J. Fluid Mech.* **87**, 417–432.

Moeng, C.-H. & Rotunno, R. 1990 Vertical-velocity skewness in the buoyancy-driven boundary layer. *J. Atmos. Sci.* **47**, 1149–1162.

Neshyba, S., Neal, V. T. & Denner, W. 1971 Temperature and conductivity measurements under upper Ice Island T-3. *J. Geophys. Res.* **76**, 8107–8120.

NOGUCHI, T. & NIINO, H. 2010 Multi-layered diffusive convection. Part 1. Spontaneous layer formation. *J. Fluid Mech.* doi:10.1017/S0022112009994150.

SCHMITT, R. W. 1994 Double diffusion in oceanography. *Annu. Rev. Fluid Mech.* **26**, 255–285.

SHIRTCLIFFE, T. G. L. 1969 An experimental investigation of thermosolutal convection at marginal stability. *J. Fluid Mech.* **35**, 677–688.

STAMP, A. P., HUGHES, G. O., NOKES, R. I. & GRIFFITHS, R. W. 1998 The coupling of waves and convection. *J. Fluid Mech.* **372**, 231–271.

TURNER, J. S. 1965 The coupled turbulent transports of salt and heat across a sharp density interface. *Intl J. Heat Mass Trans.* **8**, 759–767.

ZANGRANDO, F. & FERNANDO, H. J. S. 1991 A predictive model for the migration of double-diffusive interfaces. *J. Solar Energy Engng* **113**, 59–65.

ZIMMERMAN, W. B. & REES, J. M. 2007 Rollover instability due to double diffusion in a stably stratified cylindrical tank. *Phys. Fluids* **19**, 123604.